Optical Spectra, X-ray Photoelectron Spectra and XANES of Divalent Nickel in Mixed Spinels $NiFe_{2-x}Cr_xO_4$

M. LENGLET

Laboratoire de Physicochimie des Matériaux, INSA, BP 08, 76130 Mont-Saint-Aignan, France

A. D'HUYSSER

Laboratoire de Catalyse Hétérogène et Homogène, UA 402, UST LILLE I, 59655 Villeneuve D'Ascq Cédex, France

and C. K. JØRGENSEN

Département de Chimie Minérale Analytique et Appliquée, Université de Genève, CH-1211 Geneva 4, Switzerland

(Received January 20, 1987)

Abstract

The optical spectra, X-ray photoelectron spectra of $Ni2p_{3/2}$ and NiK-edge XANES, were measured at room temperature. The Ni^{2+} migration from octahedral to tetrahedral sites ($0.8 < x \leqslant 2$) may be correlated with the XPS and XAS parameters. Strong antiferromagnetic interactions influence the XPS Ni2p and optical spectra ($x \leqslant 1$).

Introduction

Goodenough [1] has suggested that tetrahedral Ni^{2+} sites may be stabilized by either spin-orbit or Jahn–Teller effects. If the two stabilization energies are of comparable magnitude, A-site Ni^{2+} may be stabilized by either mechanism in a spinel, depending upon the number of Ni^{2+} A-sites in the magnetic order. This author used this idea to interpret the complex properties of the system $NiFe_{2-x}Cr_xO_4$ and the crystallographic properties of the system $Cu_{1-x}Ni_xCr_xO_4$.

$NiFe_{2-x}Cr_xO_4$ has been studied crystallographically [2–4], and magnetically [5–7]. At 80 K, $NiFe_{2-x}Cr_xO_4$ shows tetragonal symmetry ($c/a > 1$) for $1.85 \leqslant x \leqslant 2$, tetragonal ($c/a < 1$) for $1.2 \leqslant x < 1.7$ and orthorhombic in the narrow intermediate range. Different magnetic structures are observed: collinear ($x \leqslant 1$), triangular ($x > 1$) [30] and conic ($NiCr_2O_4$ as proposed by Kaplan *et al.* [9]). $NiCr_2O_4$ is a cubic spinel at high temperature and becomes tetragonal below 310 K [10].

It is the purpose of the present work to establish correlations between the properties of the Ni–O chemical bond and the parameters issued from optical spectra, XPS $Ni2_p$ spectra and NiK-edge XANES, in relation with the Ni^{2+} migration in the $NiFe_{2-x}Cr_xO_4$ system.

Experimental

Optical Absorption

Figure 1 shows the visible and near-infrared diffuse reflectance spectra of different nickel ferrichromites. A study of the Ni^{2+} tetrahedral spectrum in tetragonal and cubic $NiCr_2O_4$ has already been carried out by the authors [11].

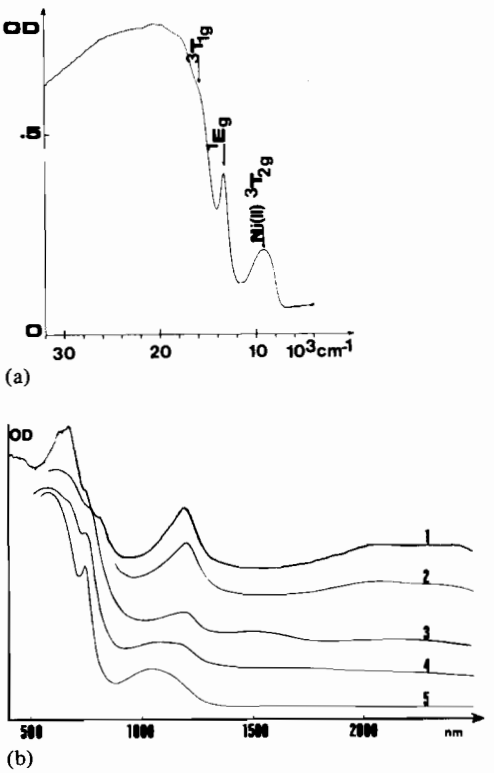

Fig. 1. Optical absorption spectra of $NiFe_{2-x}Cr_xO_4$ compounds: (a) $NiFe_2O_4$, (b) curve 1, $x = 1.9$; 2, $x = 1.6$; 3, $x = 1.2$; 4, $x = 1$; 5, $x = 0.4$.

0020-1693/87/$3.50

TABLE I. Observed Electronic Transition Energies (in kK)

	$^6A_1 \rightarrow {}^4T_1({}^4G)$	$^4T_2({}^4G)$	$^4E, {}^4A_1({}^4G)$	$^4E({}^4D)$	10 *Dq*	*B*	*C*
$ZnFe_2O_4$	8.5	12.7	20.6	24.6	14.6	0.56	3.00
α-Fe_2O_3	11.3	15.4	22.5	26.3	14.0	0.54	3.41
Fe^{3+} in T_d	14.5; 16.3	18.5; 19.6	21.6				

A complete description of the $NiFe_2O_4$ electronic spectrum requires the investigation of Fe^{3+} optical properties in ferrites.

The shape of the $ZnFe_2O_4$ (Fe^{3+} octahedrally coordinated) spectrum is identical with that of α-Fe_2O_3 (hematite) [12]. The detected band assignments are given and values of the ligand field parameters are given in Table I.

The spectrum of lithium ferrite $Li_{0.5}Fe_{2.5}O_4$ is characterized in the near infrared and visible regions by five prominent absorption bands near 10.5, 14.5, 16, 19 and 22 kK.

This sample contains 1 tetrahedrally coordinated Fe^{3+} and 1.5 octahedrally coordinated. The features at 14.5 and 19 kK can be readily assigned to the $^6A_1 \rightarrow {}^4T_1({}^4G)$ and $^6A_1 \rightarrow {}^4T_2({}^4G)$ ligand field transitions of tetrahedral Fe^{3+}. From self consistent field (SCF), Xα scattered-wave (Xα-SW) molecular orbital calculations, Sherman [13] has obtained the electronic structures of Fe^{3+} coordination sites in hematite and maghemite (trigonally distorted and octahedral $(FeO_6)^{9-}$ clusters and tetrahedral $(FeO_4)^{5-}$ cluster), and argued that the $^6A_1 \rightarrow {}^4T_1({}^4G)$ and $^6A_1 \rightarrow {}^4T_2({}^4G)$ transitions of tetrahedrally coordinated Fe^{3+} should occur near 15 and 19.5 kK in agreement with experimental data relative to Fe^{3+} in $LiAlO_2$ [14].

This study of Fe^{3+} spectra in ferrites allows the following detailed band assignments for $NiFe_2O_4$ (Table II).

TABLE II. Band Assignments for $NiFe_2O_4$

Energy (kK)	Transition		
	Ni^{2+} (O_h)	Fe^{3+}	
9.2	$^3A_{2g} \rightarrow {}^3T_{2g}$	$^6A_1 \rightarrow {}^4T_1({}^4G)$	(O_h)
13.3	$^3A_{2g} \rightarrow {}^1E_g$		
~15.5	$^3A_{2g} \rightarrow {}^3T_{1g}$		
~16.0		$^6A_1 \rightarrow {}^4T_2({}^4G)$	(O_h)
~18.1		$^6A_1 \rightarrow {}^4T_2({}^4G)$	T_d
~19.9			

The transition at 20.9 kK may be the lowest energy 'double exciton' ($^6A_1 + {}^6A_1 \rightarrow {}^4T_1({}^4G) + {}^4T_1({}^4G)$), observed on spectra of compounds in which Fe^{3+} cations are magnetically coupled to other Fe^{3+} ions [13].

Strong spin-orbit coupling together with antiferromagnetic or ferromagnetic interactions increases the intensity of the transition to the ^1E_g state near ~720–750 nm such that it becomes more intense than the spin-allowed transition to the $^3T_{1g}$ state in the case of NiO and $NiFe_2O_4$.

Spectra of the ferrimagnetic compounds in the range $0 \leqslant x \leqslant 0.8$ are characteristic of octahedral Ni^{2+}. The development of absorption at 1200 nm observed in the $NiFeCrO_4$ ($x = 1$) spectrum may be correlated with the beginning of the migration of Ni^{2+} ions from octahedral to tetrahedral sites. From reflectance spectra converted to the Kubelka–Munk remission function, it is possible to get information upon the quantity of Ni^{2+} ions on A-sites by measuring the absorption at 4.9 kK.

X-ray Photoelectron Spectroscopy

Spectra displayed in this paper were recorded using an A.E.I. ES 200 B photoelectron spectrometer. A non-monochromatized Al Kα X-ray source provided incident radiation at 1486.6 eV. Binding energies were referenced to the C1s line at 285 eV. The base pressure was 10^{-8} torr or lower.

Photoelectron spectroscopic measurements of core electrons levels in nickel compounds (and in other cations of the transition series) are complicated by 'satellite' structure located at a greater binding energy than the main or 'principal' photoemission peak. Many attempts, using a great deal of experimental information – X-ray photoemission spectroscopy [15–17], valence band photoemission, Bremstrahlung isochromat spectroscopy (BIS) [18–19], angular resolved photoemission [20], and X-ray absorption spectroscopy [21, 22] – have been made to explain these satellites in terms of ligand-to-metal charge transfer [23]. Recently, relaxation models involving screening of the XPS induced hole state have been used to account for satellites in ionic transition element compounds [24]. From an analytical point of view, it should be noted that the amplitude and exact location of satellite peaks depend critically on valence state and coordination environment of the cation and can serve as its fingerprint characterization.

In the case of the Ni^{2+} ion, measurement of the XPS parameters described on Fig. 2 allows an easy differentiation of the two species $Ni_{T_d}{}^{2+}$ and $Ni_{O_h}{}^{2+}$ in the spinel structure (Fig. 2 and Table 2 in ref. 11).

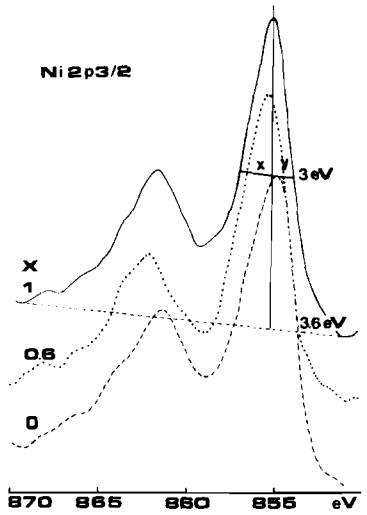

(a)

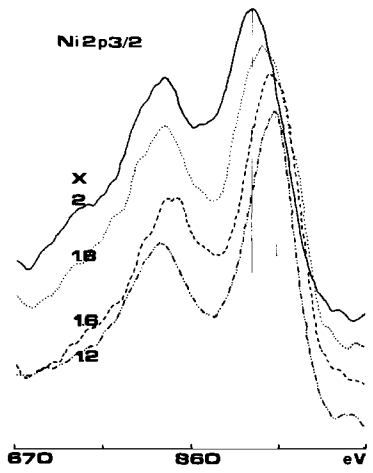

(b)

Fig. 2. XPS Ni2p spectra (a) in collinear ferrimagnetic spinels ($x \leqslant 1$) ($\alpha = x/y$); (b) for mixed spinels in the range $1 < x \leqslant 2$.

The purpose of the present work is to discover how analytically useful the measurement of these parameters can be for such compounds. This is illustrated in Fig. 2a and b which show the $Ni2p_{3/2}$ spectrum of ferrichromites $NiFe_{2-x}Cr_xO_4$ with $0 \leqslant x \leqslant 2$; Table III gives the corresponding XPS parameters. It appears that these spectra can be ordered in two ranges:

(i) In the range $0 \leqslant x \leqslant 1$ Ni^{2+} is mainly octahedral ($Ni2p_{3/2}$ binding energy and *Is/Im* values are nearly constant). The compounds are ferrimagnetic and the observed decrease in width of the $2p_{3/2}$ peak with increasing values of x is correlated with the attenuation of the magnetic interaction. A similar discussion has also been developed in the $Ni_xMg_{1-x}O$ system [25].

(ii) In the range $1 \leqslant x \leqslant 2$ the increase in the $Ni2p_{3/2}$ binding energy with increasing values of x and the variations of the XPS parameters ΔE, *Is/Im* and *FWHM* are obviously correlated with the migration of Ni^{2+} ions from B to A-sites. Points (i) and (ii) are in accordance with the optical absorption results.

X-ray Absorption Spectrometry

The K XANES of nickel and iron in ferrichromites have been performed at LURE, using synchrotron radiation emitted by the DCI storage ring in Orsay. The spectra were collected in the transmission mode.

XANES of insulating transition metal compounds can be separated into two parts:

(a) the first ~10 eV energy where the weak features called pre-edge peaks are due to transitions to unoccupied bound antibonding orbitals.

(b) the continuum part where the peaks have been identified as multiple-scattering resonances of the photoelectron sensitive to both coordination geometry and interatomic distances [26].

The Fe pre-edge fine structure in Fe(II) and Fe(III) reference compounds has been analysed as a function of coordination number. The experimental results associated with optical spectroscopic data may be interpreted by a final $Z + 1$, $(3d)^{q+1}$ configuration [27, 28]. The intensity of the prepeak allows us to estimate the 4-fold to 6-fold ratio of iron sites in spinels as $Zn_{1-x}Cu_xFe_2O_4$ [28] and $NiFe_{2-x}Cr_xO_4$ (Fig. 3, Table IV); an enhancement of the prepeak is observed for non-centrosymmetrical sites which allow the mixing of Fe-3d with oxygen-2p orbitals: the tetrahedral Fe(III) prepeak is ten times stronger than the octahedral one.

TABLE III. XPS Parameters of $Ni2p_{3/2}$ Lines in $NiFe_{2-x}Cr_xO_4$ Compounds

x	E_B (eV)	*FWHM* (eV)	α	ΔE (eV)	*Is/Im*
0	854.7	3.6	2.04	6.5	0.50
0.6	855.2	3.2	1.62	6.7	0.45
1.0	854.8	3.0	1.41	6.7	0.47
1.2	855.2	3.3		6.6	0.50
1.6	855.4	3.9		5.7	0.58
1.8	855.7	4.4		5.5	0.69
2.0	856.4	4.5		5.1	0.74

TABLE IV. XANES Parameters of Iron(III) and Nickel(II) 1_s Absorption in $NiFe_{2-x}Cr_xO_4$ Spinels

x	Fe K-edge XANES		Ni K-edge XANES							
	$Fe_{tetra}^{3+}/Fe_{octa}^{3+}$ [a]		Ni^{2+} (%) in T_d [b]			ΔE_K [c] (eV)	$E_{max} - E_{pre\text{-}edge}$		Derivative [d] spectra	
	Theoretical	Observed	(a)	(b)	(c)					
0	1.00	0.75	0		0	10.2	18.5			
0.2	1.25	1.22								
0.6	2.50	2.33								
0.8			2		0	10.2	18.6			
1.0	~9.00	9.00	15	~10	10	9.7	18.9	10.1	13.1	18.4
1.2			30		25	9.4	19.0	10.0	12.9	18.4
1.4			52	~50			19.1			
1.6			70		65	9.00	19.6	10.5	14.0	18.7
1.7				80(30)						
1.8			80		85	8.50	20.0	10.5	14.5	19.3
2.0			100		100	8.40	20.7	10.7	14.5	19.7

[a] $Fe_{tetra}^{3+}/Fe_{octa}^{3+}$ – theoretical issued from magnetic measurements; observed from XAS measurements. [b] Ni^{2+} (%) in tetrahedral coordination issued from (a) optical absorption at 4.9 kK, (b) Mössbauer and (c) X-ray absorption measurements. [c] ΔE_K chemical shift of K-edge (oxide minus metal). [d] All peak positions are taken relative to the first maximum.

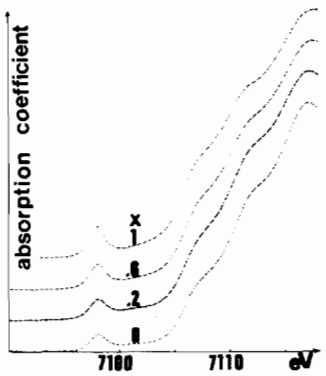

Fig. 3. Fe K-edge XANES in $NiFe_{2-x}Cr_xO_4$ ($0 \leqslant x \leqslant 1$) (all samples contain the same iron quantity).

The fine structure of Ni(II) prepeaks cannot be resolved; nevertheless, from energy and intensity measurements, it is possible to get information upon the Ni^{2+} coordination (Table IV). The tetrahedral Ni(II) prepeak is located at 0.75 eV below the octahedral prepeak and exhibits a 4–5 times enhancement.

Figure 4 shows the effect of coordination geometry on the XANES of Ni cubic spinels ($1 < x \leqslant 1.9$) in the multiple-scattering resonances range (MSR). The K-edge fine structure, disclosed by the derivative spectra, reveals the migration of Ni^{2+} ions from octahedral B-sites to tetrahedral A-sites. XANES of Cu^{2+} ions in $CuFe_2O_4$–$CuCr_2O_4$ presents an identical evolution [29]. The difference between the energy position E_{max} of the first strong maximum after the rising edge and the energy position $E_{pre\text{-}edge}$ of the transition to an antibonding state of 3d character may be equally correlated with the Ni^{2+} migration.

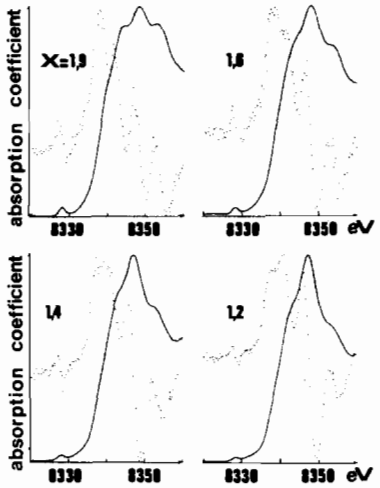

Fig. 4. Ni K-edge XANES in cubic spinels ($1 \leqslant x \leqslant 1.9$).

Conclusions

Strong antiferromagnetic interactions influence the optical spectrum and the XPS Ni2p spectrum of Ni^{2+} octahedral ions in nickel ferrichromites $NiFe_{2-x}Cr_xO_4$ ($0 \leqslant x \leqslant 1$). XPS Ni2p spectra and Ni K-edge XANES allow the differentiation of nickel species in the range $1 \leqslant x \leqslant 2$. A semi-quantitative determination of iron and nickel coordination is obtained by analysing the pre-edge peak corresponding to transitions from $1s \rightarrow 3d$-like levels on the low energy side of K-edge absorption spectra.

References

1 J. B. Goodenough, *J. Phys. Soc. Jpn.*, *17* (Suppl. B.I.), 185 (1962).

2 T. R. McGuire and S. W. Greenwald, *Solid State Phys. Electron. Telecommun., 3,* 50 (1960).
3 R. J. Arnott, A. Wold and D. R. Rogers, *J. Phys. Chem. Solids, 25,* 161 (1964).
4 P. F. Bongers, *Philips Techn. Rev., 28,* 13 (1966).
5 S. J. Pickart and R. Nathans, *Phys. Rev., 116,* 317 (1959).
6 I. S. Jacobs, *J. Phys. Chem. Solids, 15,* 54 (1960).
7 T. Tsushima, *J. Phys. Soc. Jpn., 18,* 1162 (1963).
8 A. Herpin, *Bull. Soc. Chim. Fr.,* 1094 (1965).
9 T. A. Kaplan, K. Dwight, D. Lyons and N. Menyuk, *J. Appl. Phys., 32,* 13 S (1961).
10 Y. Kino and S. Miyara, *J. Phys. Soc. Jpn., 21,* 2732 (1966).
11 M. Lenglet, A. D'Huysser, J. Arsène, J. P. Bonnelle and C. K. Jørgensen, *J. Phys. C, 19,* L363 (1986).
12 D. M. Sherman and T. D. Waite, *Am. Miner., 70,* 1262 (1985).
13 D. M. Sherman, *Phys. Chem. Miner., 12,* 161 (1985).
14 G. A. Waychunas and G. R. Rossman, *Phys. Chem. Miner., 9,* 212 (1983).
15 A. Rosencwaig, G. K. Wertheim and H. J. Guggenheim, *Phys. Rev. Lett., 27,* 479 (1971).
16 S. Hüfner and G. K. Wertheim, *Phys. Rev. B, 8,* 4857 (1973).
17 S. J. Oh, J. W. Allen, I. Lindau and J. C. Mikkelsen, *Phys. Rev. B, 26,* 4845 (1982).
18 S. Hüfner, F. Hulliger, J. Osterwalder and T. Riesterer, *Solid State Commun., 50,* 83 (1984); *52,* 793 (1984).
19 G. A. Sawatzky and J. W. Allen, *Phys. Rev. Lett., 53,* 2339 (1984).
20 J. M. McKay and V. E. Henrich, *Phys. Rev. Lett., 53,* 2343 (1984).
21 G. Van der Laan, J. Zaanen, G. A. Sawatzky, R. Karnatak and J. M. Esteva, *Solid State Commun., 56,* 673 (1985).
22 I. Davoli, A. Marcelli, A. Bianconi, M. Tomellini and M. Fanfoni, *Phys. Rev. B, 33,* 2979 (1986).
23 S. Hüfner, *Solid State Commun., 49,* 1177 (1984).
24 B. W. Veal and A. P. Paulikas, *Phys. Rev. Lett., 51,* 1995 (1983); *Phys. Rev. B, 31,* 5399 (1985).
25 M. Oku and K. Hirokawa, *J. Electron. Spectrosc., 10,* 103 (1977).
26 A. Bianconi, in 'EXAFS and near Edge Structure', Springer Series in Chemical Physics', Vol. 27, Springer, 1983, p. 118.
27 G. Calas and J. Petiau, *Solid State Commun., 48,* 625 (1983).
28 M. Lenglet, R. Guillamet, A. D'Huysser, J. Dürr and C. K. Jørgensen, 'EXAFS and Near Edge Structure IV, July 7–11, 1986', *J. Phys. Colloq. (France), 47 C-8,* 765 (1986).
29 M. Lenglet, D. Le Calonnec, J. Dürr, J. Lopitaux and J. Arsène, *Ann. Chim. Fr., 9,* 593 (1984).
30 J. Chappert and R. B. Frankel, *Phys. Rev. Lett., 19,* 570 (1967).